anthracyclines, *vinca* alkaloids, epipodophyllotoxins, taxanes, actinomycin D, mitomycin C and irinotecan [1].

We have conducted a clinical study of *MDR1* gene therapy targeting metastatic breast cancer to protect the patients' normal hematopoietic cells from toxic side-effects during post-transplantation chemotherapy. Two patients (patients 1 and 2) received high-dose chemotherapy and a transplantation of HaMDR retrovirus-transduced CD34+ cells in 2001. They subsequently underwent post-transplantation docetaxel chemotherapy. These patients entered complete remission in 2001, and the remission lasted for 3–5 years. In patient 1, the *MDR1* transgene was found to be present in the peripheral blood mononuclear cells obtained during the initial recovery phase after transplantation (days 12 and 40). The transgene levels were then observed to decrease gradually, however, with the lowest levels on day 257. This patient received ten cycles of docetaxel chemotherapy on days 71–316. On day 327, the *MDR1* transgene levels were observed to have increased again, with the highest levels detectable on day 439, yet they were undetectable by day 1461. The estimated proportions of gene-modified cells on days 40, 257 and 439 were 1%, 0.01% and 1%, respectively. By contrast, in patient 2, the *MDR1*-transduced cells decreased within 1 month, and *MDR1* transgene-positive cells were detected only occasionally [2,3]. A third patient received the transplantation in 2004, and was treated with various chemotherapy protocols because of progressive diseases.

Studies of retrovirus-mediated hematopoietic stem cell (HSC) gene therapy have been conducted for the treatment of X-linked severe combined immunodeficiency (X-SCID), adenosine deaminase (ADA) deficiency, X-linked chronic granulomatous disease (X-CGD) and others. Among these treatments, clinical benefits have been demonstrated in the treatment of X-SCID and ADA-SCID [4–10]. However, five X-SCID patients developed T cell leukemia 2–5 years after the transplantations. In four patients, the retroviral integration in blast cells were near the *LIM domain only 2* (*LMO2*) proto-oncogene, and, in the other patient, the blast cells showed an integration near *cyclin D2* (*CCND2*). This suggests that the retroviral integration activated these genes, thereby promoting clonal T cell proliferation [11–13]. Subsequent to the reports of these adverse events, retroviral insertional mutagenesis has become a serious concern regarding the safety of HSC gene therapy [14].

We previously reported the engraftment, docetaxel-induced amplification and persistence of *MDR1* transgene-positive cells in the peripheral blood of the first two patients who received the transplantation in 2001, after a 6-year follow-up [3]. By linear-amplification-mediated polymerase chain reaction (LAM-PCR) and subsequent clone-specific PCR, we identified four long-life clones that appeared in the peripheral blood of patient 1 between days 300 and 1300 after the transplantation. *In vivo* amplification of these clones occurred after ten cycles of docetaxel treatment, and the profiles of the amplification and disappearance of these clones were similar to those of the total *MDR1*-transduced cells of the patient. One of these clones had a retroviral integration upstream of *ecotropic viral integration site 1* (*EVI1*), although the other three did not show integration near genes known to be responsible for lymphoproliferation.

In the present study, we report the retroviral integration site analysis of patient 3, who received the transplantation in 2004 in our *MDR1* gene therapy program.

Materials and methods

Clinical procedures

The HaMDR retrovirus used in the present study carries a wild-type (Gly185) *MDR1* cDNA insert in the Harvey sarcoma virus backbone [15–17]. A HaMDR producer clone 3P26, with a retrovirus titer of 10^7 cfu/ml, was established in our laboratory. The clinical grade HaMDR retrovirus was prepared by MAGENTA (Rockville, MD, USA). The clinical grade human cytokines, stem cell factor, FMS-like tyrosine kinase 3 ligand, soluble interleukin (IL)-6 receptor and thrombopoietin, were obtained from R&D Systems (Minneapolis, MN, USA). GMP grade human IL-6 was a generous gift from Serono Japan (Tokyo, Japan). Our clinical protocol for *MDR1* gene therapy was approved by the Japanese government in February 2000. Briefly, advanced or recurrent breast cancer patients who responded well to conventional induction chemotherapy were enrolled in this protocol. After obtaining informed consent, patients were treated with 2 g/m^2 cyclophosphamide on day 1, and then with 300 μg/day granulocyte colony-stimulating factor on days 10–15. Peripheral blood mononuclear cells were harvested on days 13–15. Cells harvested on days 13 and 15 were cryopreserved without any modification until transplantation. CD34+ cells were separated from the cells harvested on day 14 by magnetic microbead selection using an Isolex 50 Stem Cell Reagent kit (Nexell Therapeutics Inc., Irvine, CA, USA). The purified CD34+ cells were subsequently cultured in medium containing 50 ng/ml stem cell factor, 100 ng/ml FMS-like tyrosine kinase 3 ligand, 300 ng/ml soluble IL-6 receptor, 20 ng/ml thrombopoietin and 100 ng/ml IL-6. Thirty-six hours after the initiation of the *ex vivo* cultures, the cells were transduced with HaMDR retrovirus on plates coated with CH-296 (Takara Bio Inc, Otsu, Japan) for 4 h, on three occasions over a 36-h period. The cells were then washed and cryopreserved. After the biosafety tests on the transduced cells had been completed, the patients received high-dose chemotherapy of 2 g/m^2 cyclophosphamide, 67 mg/m^2 thiotepa and 533 mg/m^2 carboplatin daily for 3 days. Three days after the completion of the high-dose chemotherapy, the *MDR1*-transduced CD34+ cells were reinfused together with the unmodified cells. After their bone marrow function had recovered, the patients received post-transplantation chemotherapy.

MDR1 PCR

Genomic DNA extracted from peripheral blood mononuclear cells was preamplified using a GenomiPhi DNA amplification kit (Amersham Biosciences, Piscataway, NJ, USA). HaMDR proviral DNA (100 ng/reaction) was amplified using the primers 5′-ATAGGGGTTTTTACAAGAAT-3′ and 5′-AGCATAGGAAAAATACATCA-3′. β-globin was amplified as an internal control with the primers 5′-G AAGAGCCAAGGACAGGTAC-3′ and 5′-CATCAGGAGTG GACAGATCC-3′.

LAM-PCR

The retroviral integration loci of the *MDR1*-transduced cells were amplified by LAM-PCR as described previously [3]. First, the genomic-proviral junction sequence was preamplified by 50 cycles of primer extension using 0.25 pmol of the HaMDR vector-specific, 5′-biotinylated primer LTR11 (5′-AGCTGTTCTATCTGTTCTTGGCCCT-3′), AccuPrime Taq DNA polymerase (Invitrogen, Carlsbad, CA, USA) and 100 ng of each DNA sample. The resulting products were purified using a μMACS Streptavidin Kit (Miltenyi Biotec, Bergisch Gladbach, Germany). The products linked to the magnetic beads were next incubated with a random hexanucleotide mixture (Roche Diagnostics, Mannheim, Germany) and 4.4 U of Klenow polymerase (Invitrogen) at 37 °C for 1 h, washed using a magnetic particle concentrator and then digested with 5 U of *Mae*II endonuclease (Roche Diagnostics) at 50 °C for 1 h. After an additional washing step, the LAM-PCR products were ligated to 100 pmol of a double-stranded asymmetric linker cassette consisting of Linker4+ (5′-GACCCGGGAGATCTGAATTCAGTGGCACAGCA-3′) and Linker4− (5′-CGTGCTGTGCCACTGAATTCAGATCTCCCG GGTC-3′). The ligation products were purified using a magnetic particle concentrator and then amplified by PCR with the vector-specific primer LTR2 (5′-GACCTTGATCTGAACTTCTC-3′) and the linker cassette primer LC11 (5′-GACCCGGGAGATCTGAATTC-3′). The PCR products then served as templates for a second, nested PCR using the internal primers LTR31 (5′-TCCATGCCTTGTAAAATGGC-3′) and LC12 (5′-GATCTGAATTCAGTGGCACAG-3′) with the same cycling conditions. LAM-PCR products were subcloned and then sequenced. The HaMDR proviral integration sites were identified using the NCBI BLASTN Database (http://ncbi.nih.gov/BLAST/). Genes located less than 500 kb from the proviral integration site were identified for each clone. We then examined whether these genes were homologous to any of the murine retroviral common integration sites defined in the Retroviral Tagged Cancer Gene (RTCG) Database (http://rtcgd.ncifcrf.gov).

Clone-specific PCR

Clone-specific PCR was performed with the vector-specific primers and the appropriate clone-specific primers. The vector-genome junctions of clones N-30 and N-31 were amplified using nested PCR. The first PCR for N-30 was carried out using the primers P30−1 (5′-CACACTTTCCAGCCCCTCTT-3′) and LTR3386 (5′-AGCGAGAAGCGAACTGATTG-3′), and the second PCR was performed with the primers P30-2 (5′-CCCTCTTGCCCCACCTCTCC-3′) and LTR3355 (5′-T AAGGCACAGGGTCATTTCA-3′). The first PCR for N-31 was carried out using the primers P31-1 (5′-AGGGGGT CTGTTTCATTCTG-3′) and LTR3386, and the second PCR was performed with the primers P31-2 (5′-ATAGGGTAAAGGTAGTTGTG-3′) and LTR3355. The internal control PCR reaction for β-globin was performed as described above.

Results

PCR analysis of the *MDR1* transgene-positive cells in the peripheral blood

Patient 3 received a transplantation of the *MDR1*-transduced, P-gp-positive cells (2.6×10^5/ kg), which was 2.9% of the total reinfused CD34+ cells (9.4×10^6/ kg), in August 2004. This patient did not enter complete remission after high-dose chemotherapy, and received four regimens of post-transplantation chemotherapy over 2 years, as shown in Table 1. Serial peripheral blood samples were obtained between days 12 and 831 and were tested for the presence of the *MDR1* transgene by PCR amplification of the DNA (Figure 1). The *MDR1* transgene was present in the peripheral blood mononuclear cells obtained on day 12, in the initial recovery phase after transplantation. The transgene levels then decreased and remained low until day 385. A slight increase in the levels of the *MDR1* transgene was observed between days 160 and 210, when the patient received the vinorelbine treatment (Table 1). On day 448, the level of the *MDR1* transgene started to increase again. On day 532, the level became higher than that on day 12. This high level was maintained until day 831. This patient received combination chemotherapy with mitomycin C and methotrexate between days 336 and 649. The estimated proportions of gene-modified cells on days 12, 336, 532 and 686 were 1%, 0.1%, 1% and 5%, respectively, as assessed by PCR on serial dilutions of peripheral blood DNA (data not shown). This patient died of progressive liver metastasis of the breast cancer on day 851. No blast cells were detected in the peripheral blood of the patient throughout the observation period.

Identification of HaMDR integration sites by LAM-PCR

LAM-PCR was performed to isolate the vector-genome junctions of the *MDR1*-transduced circulating leukocyte clones from patient 3. On the basis of the results of the

Table 1. Post-transplantation chemotherapy for patient 3

Regimen	Cycles	Dose	Start day of each cycle (days after transplantation)
VNB[a] (28-day cycle)	1	vinorelbine; 12.5 mg/m^2 on days 1, 8, 15	76
	2–5	vinorelbine; 18.75 mg/m^2 on days 1, 8, 15	104, 132, 167, 201[b]
CAP (28-day cycle)	1–4	capecitabine; 1600 mg/m^2 on days 1–21	217, 252, 280, 308
MMC + MTX (28-day cycle)	1–8	mitomycin C; 8 mg/m^2 on day 1 and methotrexate; 60 mg/m^2 on days 1, 15	336, 371, 399, 434, 490, 553, 595, 649[c]
TS-1 (35-day cycle)	1–2	TS-1; 66.7 mg/m^2 on days 1–28	714[d], 768[e]

[a]VNB, vinorelbine; CAP, capecitabine; MMC, mitomycin C; MTX, methotrexate; TS-1, a mixture of tegafur and two modulators, 5-chloro-2,4-dihydroxypyrimidine and potassium oxonate. [b]In the fifth cycle of VNB, vinorelbine was administered on day 201 only. [c]In the eighth cycle of MMC + MTX, mitomycin C and methotrexate were administered on day 649, but the second methotrexate was not administered. [d]In the first cycle of TS-1, the drug was given on days 714–719 and 736–754. [e]In the second cycle of TS-1, the drug was given on days 768–788.

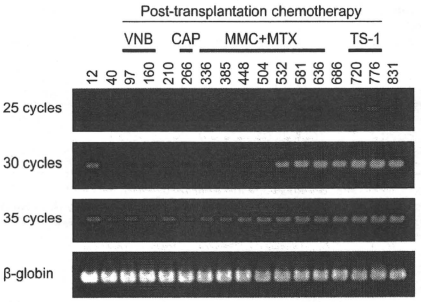

Figure 1. PCR analysis of the *MDR1* transgene in the peripheral blood mononuclear cells of patient 3. Peripheral blood samples were obtained on the indicated days post-transplantation and genomic DNA extracted from these preparations was preamplified with a GenomiPhi DNA Amplification Kit. HaMDR proviral DNA (100 ng/reaction) was amplified by PCR with AmpliTaq Gold DNA polymerase using 25, 30 or 35 cycles. An equal amount of DNA from each sample was amplified using β-globin-specific primers as an internal control. PCR products were analyzed on 2.5% agarose gels. Post-transplantation chemotherapy is indicated above: VNB, vinorelbine; CAP, capecitabine; MMC, mitomycin C; MTX, methotrexate; TS-1, a mixture of tegafur and two modulators, 5-chloro-2,4-dihydroxypyrimidine and potassium oxonate

MDR1 DNA PCR, we selected six DNA samples obtained on days 12, 504, 581, 679, 686 and 831, and performed LAM-PCR. Thirty-one independent vector-genome junctions were identified. We assumed that these junctions were isolated from independent clones and denoted them N-1 to N-31. Among the 31 clones, 23 were isolated from the blood sample taken on day 12. We referred to these as short-life clones. The remaining eight clones were isolated from DNA samples obtained on day 504 or later. These clones were referred to as long-life clones. Three long-life clones (N-24, N-25 and N-26) were also isolated on day 12. Table 2 shows the analysis of the integration site for the long-life clones. Analysis of the integration site for the short-life clones is shown in the Supporting information (Table S1).

RTCGs located near HaMDR integration sites

Table 3 lists the *MDR1*-transduced clones for which proviral integration occurred within 500 kb of RTCGs. These clones are denoted as RTCGD-hit clones. The positions and orientations of the RTCGs, together with the genes present within a 500-kb region around the retroviral integration sites of the ten RTCGD-hit clones, are represented schematically in Figure 2. Two clones, N-30 and N-31, had HaMDR integrations in the promoter region of *EVI1*. The distances from the integration sites to the transcriptional start site (TSS) of *EVI1* in N-30 and N-31 were 0.7 kb and 94 kb, respectively. Clones N-28 and N-29 showed HaMDR integrations within intron 1 of the RTCGs, *PRDM16* and *CUEDC1*, respectively. N-13 had a HaMDR integration 298 kb upstream of *GNA12*. N-12 showed an integration within intron 52 of *DST*. In the remaining four RTCGD-hit clones, N-1, N-2, N-8 and N-17, three or more genes were present between the HaMDR proviral integration site and the RTCG. Six RTCGD-hit clones (N-1, N-2, N-8, N-12, N-13 and N-17) were short-life clones isolated from the blood sample taken on day 12 and were not detected again, even after the patient received multiple rounds of chemotherapy. The other four RTCGD-hit clones (N-28, N-29, N-30 and N-31) were long-life clones isolated from the blood sample taken on day 504 or later.

Expansion of clones with retroviral integration upstream of *EVI1*

Among the eight long-life clones, two clones, N-30 and N-31, had retroviral insertion sites within the promoter region of *EVI1*. We previously reported a long-life clone from patient 1, L-34, which had a retroviral integration site 179 kb upstream of *EVI1* (Figure 3A). We therefore carried out clone-specific PCR to evaluate the persistence, possible expansion and fate of these two clones. Eighteen peripheral leukocyte DNA samples from patient 3 were selected and subjected to clone-specific PCR. As shown in Figure 3B, N-30 was detected in the blood samples between days 636 and 776. In N-31, weak signals for this clone were detectable in the blood samples taken on days

DOI: 10.1002/jgm

Table 2. HaMDR integration site analysis of long-life clones

Clone	Days after transplantation	Integration site: Locus (bp)	Integration site: Chromosome	Gene of interest: Comment	Gene of interest: Gene name[a]	Provirus: Position[b]	Provirus: Distance (kb) from TSS[c]	Provirus: Orientation[d]
N-24	12, 504	25 954853	1p35	In gene	*MAN1C1*	Intron 5	138	Same
				5′-nearest	*LDLRAP1*	D	212	Same
				3′-nearest	*SEPN1*	U	44	Same
N-25	12, 686, 831	190 752337	1q31	5′-nearest	*RGS1*	U	59	Opposite
				3′-nearest	*RGS21*	D	200	Opposite
N-26	12, 686, 831	17 337587	3p24	In gene	*TBC1D5*	Intron 13	420	Same
				5′-nearest	None	–	–	–
				3′-nearest	*PLCL2*	D	388	Opposite
N-27	581	135 674371	Xq26	In gene	*ARHGEF6*	Intron 2	16	Opposite
				5′-nearest	*CD40LG*	U	116	Same
				3′-nearest	*RBMX*	D	116	Opposite
N-28	679	3089 013	1p36	In gene and RTCG	***PRDM16*** (8)	Intron 1	113	Opposite
				5′-nearest	*ARHGEF16*	U	280	Opposite
				3′-nearest	*ACTRT2*	D	161	Opposite
N-29	686	53 332944	17q22	In gene and RTCG	***CUEDC1*** (3)	Intron 1	2	Opposite
				5′-nearest	*LOC100128440*	D	40	Same
				3′-nearest	*VEZF1*	D	87	Opposite
N-30	831	170 348998	3q26	5′-nearest	*MDS1*	D	515	Same
				3′-nearest and RTCG	***EVI1*** (7)	U	0.7	Same
N-31	504, 581, 679, 686, 831	170 441489	3q26	In gene	*MDS1*	Intron 2	423	Same
				5′-nearest	*LOC730004*	D	243	Same
				3′-nearest and RTCG	***EVI1*** (7)	U	94	Same

RTCG, retroviral tagged cancer gene. [a]Genes listed in the Retroviral Tagged Cancer Gene Database are shown in bold, and their frequency in this database is indicated in parentheses. [b]Position of the provirus with respect to the gene (U, provirus integrated upstream of the gene; D, provirus integrated downstream of the gene). [c]TSS, transcriptional start site. [d]Orientation of the inserted provirus in relation to the gene (same, provirus in same orientation as the gene; opposite, provirus in opposite orientation to the gene).

Table 3. HaMDR integration site analysis of RTCGD-hit clones

Clone	Days after transplantation	Integration site: Locusc (bp)	Integration site: Chromosome	Gene of interest: Comment	Gene of interest: Gene name[a]	Provirus: Position[b]	Provirus: Distance (kb) from TSS[c]	Provirus: Orientation[d]
N-1	12	23 369443	1p36	RTCG	***E2F2*** (10)	D	361	Same
				RTCG	***ID3*** (10)	D	389	Same
N-2	12	152 029382	1q21	RTCG	***S100A14*** (2)	U	174	Same
N-8	12	43 070866	5p13	RTCG	***GHR*** (6)	D	611	Same
N-12	12	56 514753	6p12	In gene and RTCG	***DST*** (2)	Intron 52	412	Same
N-13	12	3148 350	7p22	RTCG	***GNA12*** (4)	U	298	Same
N-17	12	104 611982	14q32	RTCG	***AKT1*** (6)	U	279	Same
				RTCG	***CRIP2*** (4)	U	400	Opposite
N-28	679	3089 013	1p36	In gene and RTCG	***PRDM16*** (8)	Intron 1	113	Opposite
N-29	686	53 332944	17q22	In gene and RTCG	***CUEDC1*** (3)	Intron 1	2	Opposite
N-30	831	170 348998	3q26	3′-nearest and RTCG	***EVI1*** (7)	U	0.7	Same
N-31	504, 581, 679, 686, 831	170 441489	3q26	3′-nearest and RTCG	***EVI1*** (7)	U	94	Same

RTCG, retroviral tagged cancer gene. [a]Genes listed in the Retroviral Tagged Cancer Gene Database are shown in bold, and their frequency in this database is indicated in parentheses. [b]Position of the provirus with respect to the gene (U, provirus integrated upstream of the gene; D, provirus integrated downstream of the gene). [c]TSS, transcriptional start site. [d]Orientation of the inserted provirus in relation to the gene (same, provirus in same orientation as the gene; opposite, provirus in opposite orientation to the gene).

97 and 160, but were undetectable on days 210 and 266. On day 336, N-31 began to increase. Between days 679 and 831, the signals for N-31 were almost consistently strong. This pattern was similar to that of the *MDR1* PCR.

Discussion

We have demonstrated the engraftment and persistence of *MDR1* transgene-positive cells in the peripheral blood of a patient in our *MDR1* gene therapy program. The *MDR1* transgene was initially present in the peripheral blood 12 days after the transplantation, but decreased to low levels until day 504. Then, a remarkable increase in *MDR1* transgene-positive cells was observed on day 532, in the middle of the combination chemotherapy regimen of mitomycin C and methotrexate. Using LAM-PCR, we identified eight long-life clones that survived for more than 500 days after the transplantation. Among them, two clones, N-30 and N-31, had retroviral integrations within the *EVI1* locus. *In vivo* amplification of N-31 also occurred during combination chemotherapy with mitomycin C and

DOI: 10.1002/jgm

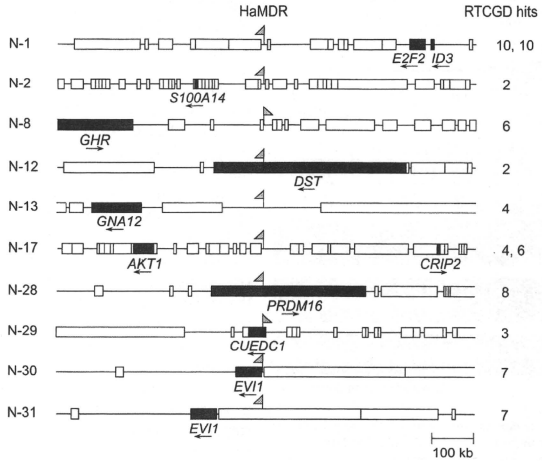

Figure 2. Schematic representation of the HaMDR integration sites and their neighboring RTCGs, together with their orientations in the RTCGD-hit clones. RTCGs within the 500-kb region around the retroviral integration sites are shown. The HaMDR proviral insertion sites are indicated by the triangular flags. The direction of the flag indicates the orientation of the provirus. RTCGs are indicated by filled bars; other genes are denoted using open bars. The orientation of each RTCG is indicated by an arrow

methotrexate, and the profile of the amplification and disappearance of this clone was similar to that of the total *MDR1*-transduced cells in the patient. This patient died of progressive disease 28 months after transplantation. No blast cells were detected in the peripheral blood of the patient throughout the observation period.

There have been several reports in which the effects of anticancer agents were evaluated as the underlying cause of the expansion of the *MDR1*-transduced cells in the patients' peripheral blood. In a study conducted at the National Cancer Institute (Bethesda, MD, USA), a successful enrichment of *MDR1*-transduced hematopoietic cells was demonstrated following chemotherapy with paclitaxel or doxorubicin [18]. Another study demonstrated etoposide-dependent enrichment of *MDR1*-transduced hematopoietic cells [19]. In a previous study, we have also shown that *MDR1*-transduced cells were enriched by docetaxel [3]. These results suggest that transduced *MDR1* gene could confer resistance against such chemotherapeutic drugs in peripheral leukocytes *in vivo*. In the present study, we show that the combination chemotherapy of mitomycin C and methotrexate could also expand *MDR1*-transduced cells *in vivo*. Mitomycin C is one of the substrates of P-gp, and *MDR1*-transduced cells showed cross-resistance to mitomycin C [20]. By contrast, methotrexate is not a good substrate of P-gp. Taken together, we conclude that the transduced *MDR1* gene conferred resistance to mitomycin C in the peripheral leukocytes *in vivo*. It is difficult to comment on whether the expansion of gene-modified cells was of clinical relevance for the patient in terms of white blood cell count recovery after the chemotherapy cycles. The data obtained from only three patients are insufficient to show whether *MDR1* transduction of the peripheral blood CD34+ cells protected hematopoietic cells from the toxicity of the chemotherapeutic agents. In addition, in the present study, only one-third of the harvested CD34+ cells were transduced with the *MDR1* vector; two thirds were returned to the patient without genetic modification to ensure the bone marrow engraftment after high-dose chemotherapy. This reduced the ratio of *MDR1*-transduced cells compared to total reinfused CD34+ cells. However, comparison of patient 1 and patient 2, in whom the white blood cells from the former had a higher proportion of P-gp-positive cells compared to those from the latter, showed that a higher proportion of P-gp-positive cells might correlate with reduced bone marrow toxicity [2]. This suggests a possible use for the gene-modified cells. Future studies with more efficient transduction protocols will be necessary to clarify this point.

We have identified 38 clones from patient 1 and 31 clones from patient 3 [3]. Among them, clones with retroviral integration in the *MDS1 and EVI1 complex locus* (*MECOM*) were most frequently isolated. A long-life clone from patient 1, L-34, had a retroviral integration 179 kb upstream of *EVI1* [3]. Two long-life clones from patient 3, N-30 and N-31, had HaMDR integrations 0.7 kb and 94 kb upstream of *EVI1*, respectively. It should be noted that all of these three clones were long-life clones. L-34 was expanded in the peripheral blood between days 327 and 1154, and then disappeared. N-31 began to increase on day 336 and was consistently high until day

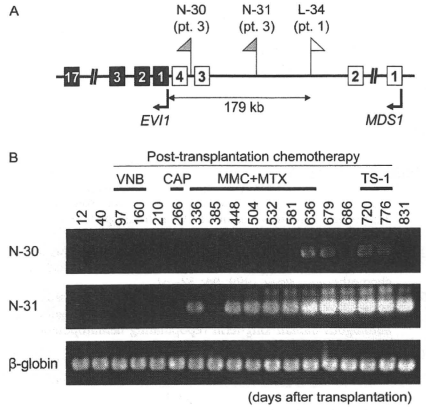

Figure 3. Expansion of clones with retroviral integration in the *MDS1 and EVI1 complex locus* (*MECOM*). (A) Location of the three independent retroviral integration sites identified in the *MECOM*. The triangular flags indicate the retroviral integration sites of each clone. L-34 is a clone isolated from patient 1 [3]. Open and closed boxes with numbers indicate exons of *MDS1* and *EVI1*, respectively. The figure is not shown to scale (pt, patient). (B) Clone-specific PCR amplification of the vector-genome junctions in mononuclear cells obtained from the peripheral blood of patient 3. Peripheral blood was harvested from patient 3 at the indicated time-points between 12 and 831 days post-transplantation. Genomic DNA samples extracted from these mononuclear cells were preamplified with GenomiPhi DNA Amplification Kit. HaMDR proviral DNA (100 ng/reaction) was amplified by PCR, using a vector-specific primer and the appropriate clone-specific primer, as described in the Materials and methods. An equal amount of DNA from each sample was amplified using the β-globin-specific primers as an internal control. PCR products were analyzed on 2.5% agarose gels. Post-transplantation chemotherapy is indicated above: VNB, vinorelbine; CAP, capecitabine; MMC, mitomycin C; MTX, methotrexate; TS-1, a mixture of tegafur and two modulators, 5-chloro-2,4-dihydroxypyrimidine and potassium oxonate

831. By contrast, N-30 was detected only at marginal levels in patient 3. In a gene therapy trial for X-CGD, *MECOM* was recognized as the most frequently identified retroviral integration site in clones that persisted in the long term in the patients' peripheral blood [10]. The most productive clone in a patient had an insertion approximately 210 kb upstream of *EVI1*. Its quantitative contribution to the pool of transduced cells increased from day 122 onward, peaking on day 381 at approximately 80% of gene-modified cells present in the peripheral blood, and remaining at that level until the last time-point analyzed, on day 542. In another HSC gene therapy study using rhesus macaques, 14 clones with retrovirus insertions in the *MECOM* were identified in nine animals. Among these 14 clones, 11 had integrations upstream of *EVI1*. These clones were observed to be stable over the long term, primarily in myeloid cells. All of these animals were hematologically normal, without evidence of leukemia [21].

Among the eight long-life clones we identified from patient 3, clones N-28 and N-29 showed HaMDR integrations within intron 1 of *PRDM16* and *CUEDC1*, respectively. In a study of X-CGD, intron 1 of *PRDM16* was identified as another frequently observed retroviral integration site, and a region 112–115 kb downstream of the TSS was the hotspot for integration [10]. *PRDM16* is another candidate gene that facilitates long-term survival of the transduced clones. The other four long-life clones from patient 3 (N-24, N-25, N-26 and N-27) were not RTCGD-hit clones. It should be noted that three of them (N-24, N-25 and N-26) were isolated on day 12, during the initial recovery phase. Clones identifiable at both early and late time-points might be related to the abundance of these clones in the peripheral blood of the patients. Insertional mutagenesis induced by *MDR1* gene transfer has been studied in animal models. The occurrence of a polyclonal myeloproliferative syndrome in mice after transplantation of marrow cells transduced with HaMDR was shown to be the result of retroviral insertional mutagenesis [22,23]. In a primate model, no evidence of clonal dominance of *MDR1*-transduced marrow cells was observed in a 4-year follow-up study [24].

In our clinical study of *MDR1* gene therapy, we evaluated three recurrent breast cancer patients who had developed metastases: patient 1 in the lung, patient 2 in the lymph nodes and patient 3 in the liver. Patients 2 and 3 died 92 and 28 months, respectively, after high-dose chemotherapy. Patient 1 has been alive for more than 8 years in stable condition. There has been no indication of abnormal proliferation of *MDR1*-transduced clones. In conclusion, the present study suggests that *MDR1*-transduced cells were enriched *in vivo* by mitomycin C, and the possible activation of *EVI1* or other RTCGs by retroviral insertion may have affected the survival and persistence of a proportion of the transduced cells.

Supporting Information

Table S1. HaMDR integration site analysis of short-life clones

Acknowledgements

This work was supported in part by grants from the Ministry of Education, Culture, Sports, Science and Technology, Japan; the Ministry of Health, Labour and Welfare, Japan; and the Nippon Foundation, Japan. The authors declare that they have no competing interests.

References

1. Gottesman MM, Pastan I. Biochemistry of mutidrug resistance mediated by the multidrug transporter. *Annu Rev Biochem* 1993; **62**: 385–427.

2. Takahashi S, Aiba K, Ito Y, *et al.* *MDR1* gene transfer into hematopoietic stem cells and maintenance of transduced leukocytes by docetaxel chemotherapy in metastatic breast cancer patients. *Cancer Sci* 2007; **10**: 1609–1616.
3. Mitsuhashi J, Tsukahara S, Suzuki R, *et al.* Retroviral integration site analysis and the fate of transduced clones in an *MDR1* gene therapy protocol targeting metastatic breast cancer. *Hum Gene Ther* 2007; **18**: 895–906.
4. Blaese RM, Culver KW, Chang L, *et al.* Treatment of severe combined immunodeficiency disease (SCID) due to adenosine deaminase deficiency with CD34+ selected autologous peripheral blood cells transduced with a human ADA gene. Amendment to clinical research project. Project 90-C-195, January 10, 1992. *Hum Gene Ther* 1993; **4**: 521–527.
5. Malech HL, Maples PB, Whiting-Theobald N, *et al.* Prolonged production of NADPH oxidase-corrected granulocytes after gene therapy of chronic granulomatous disease. *Proc Natl Acad Sci USA* 1997; **94**: 12133–12138.
6. Cavazzana-Calvo M, Hacein-Bey S, De Saint Basile G, *et al.* Gene therapy of human severe combined immunodeficiency (SCID)-X1 disease. *Science* 2000; **288**: 669–672.
7. Aiuti A, Slavin S, Aker M, *et al.* Correction of ADA-SCID by stem cell gene therapy combined with nonmyeloablative conditioning. *Science* 2002; **296**: 2410–2413.
8. Hacein-Bey-Abina S, Le Deist F, Carlier F, *et al.* Sustained correction of X-linked severe combined immunodeficiency by ex vivo gene therapy. *N Engl J Med* 2002; **346**: 1185–1193.
9. Gaspar HB, Parsley KL, Howe S, *et al.* Gene therapy of X-linked severe combined immunodeficiency by use of a pseudotyped gammaretroviral vector. *Lancet* 2004; **364**: 2181–2187.
10. Ott MG, Schmidt M, Schwarzwaelder K, *et al.* Correction of X-linked chronic granulomatous disease by gene therapy, augmented by insertional activation of *MDS1-EVI1, PRDM16* or *SETBP1*. *Nat Med* 2006; **12**: 401–409.
11. Hacein-Bey-Abina S, von Kalle C, Schmidt M, *et al.* *LMO2*-associated clonal T cell proliferation in two patients after gene therapy for SCID-X1. *Science* 2003; **302**: 415–419.
12. McCormack MP, Rabbitts TH. Activation of the T-cell oncogene *LMO2* after gene therapy for X-linked severe combined immunodeficiency. *N Engl J Med* 2004; **350**: 913–922.
13. Hacein-Bey-Abina S, Garrigue A, Wang GP, *et al.* Insertional oncogenesis in 4 patients after retrovirus-mediated gene therapy of SCID-X1. *J Clin Invest* 2008; **118**: 3132–3142.
14. Kohn DB, Sadelain M, Dunbar C, *et al.* American Society of Gene Therapy (ASGT) ad hoc subcommittee on retroviral-mediated gene transfer to hematopoietic stem cells. *Mol Ther* 2003; **8**: 180–187.
15. Kioka N, Tsubota J, Kakehi Y, *et al.* P-glycoprotein gene (MDR1) cDNA from human adrenal: normal P-glycoprotein carries Gly185 with an altered pattern of multidrug resistance. *Biochem Biophys Res Commun* 1989; **162**: 224–231.
16. Hibino H, Tani K, Ikebuchi K, *et al.* The common marmoset as a target preclinical primate model for cytokine and gene therapy studies. *Blood* 1999; **93**: 2839–2848.
17. Sugimoto Y, Tsukahara S, Sato S, *et al.* Drug-selected co-expression of P-glycoprotein and gp91 in vivo from an *MDR1*-bicistronic retrovirus vector Ha-MDR-IRES-gp91. *J Gene Med* 2003; **5**: 366–376.
18. Moscow JA, Huang H, Carter C, *et al.* Engraftment of *MDR1* and NeoR gene-transduced hematopoietic cells after breast cancer chemotherapy. *Blood* 1999; **94**: 52–61.
19. Abonour R, Williams DA, Einhorn L, *et al.* Efficient retrovirus-mediated transfer of the multidrug resistance 1 gene into autologous human long-term repopulating hematopoietic stem cells. *Nat Med* 2000; **6**: 652–658.
20. Yusa K, Sato W, Yamazaki A, Tsukahara S, Tsuruo T. Cross-resistance of human multidrug-resistant cells to mitomycin C. *Anticancer Res* 1991; **11**: 1301–1304.
21. Calmels B, Ferguson C, Laukkanen MO, *et al.* Recurrent retroviral vector integration at the *Mds1/Evi1* locus in nonhuman primate hematopoietic cells. *Blood* 2005; **106**: 2530–2533.
22. Bunting KD, Galipeau J, Topham D, Benaim E, Sorrentino BP. Transduction of murine bone marrow cells with an *MDR1* vector enables ex vivo stem cell expansion, but these expanded grafts cause a myeloproliferative syndrome in transplanted mice. *Blood* 1998; **92**: 2269–2279.
23. Modlich U, Kustikova OS, Schmidt M. Leukemias following retroviral transfer of multidrug resistance 1 (*MDR1*) are driven by combinatorial insertional mutagenesis. *Blood* 2005; **105**: 4235–4246.
24. Bozorgmehr F, Laufs S, Sellers SE. No evidence of clonal dominance in primates up to 4 years following transplantation of multidrug resistance 1 retrovirally transduced long-term repopulating cells. *Stem Cells* 2007; **25**: 2610–2618.

FEBS Letters 584 (2010) 3885–3890

ELSEVIER

FEBS Letters

journal homepage: www.FEBSLetters.org

Tankyrase-1 assembly to large protein complexes blocks its telomeric function

Kaori Hatsugai [a,b], Tomokazu Ohishi [a], Yoshikazu Sugimoto [b,c], Hiroyuki Seimiya [a,*]

[a] Division of Molecular Biotherapy, Cancer Chemotherapy Center, Japanese Foundation for Cancer Research, 3-8-31 Ariake, Koto-ku, Tokyo 135-8550, Japan
[b] Division of Chemotherapy, Faculty of Pharmacy, Keio University, 1-5-30 Shiba-Koen, Minato-ku, Tokyo 105-8512, Japan
[c] Division of Gene Therapy, Cancer Chemotherapy Center, Japanese Foundation for Cancer Research, 3-8-31 Ariake, Koto-ku, Tokyo 135-8550, Japan

ARTICLE INFO

Article history:
Received 1 July 2010
Revised 27 July 2010
Accepted 29 July 2010
Available online 7 August 2010

Edited by Varda Rotter

Keywords:
Telomere
Tankyrase-1
Poly(ADP-ribose) polymerase
TRF1

ABSTRACT

Tankyrase-1 poly(ADP-ribosyl)ates the telomere-binding protein TRF1. This post-translational modification dissociates TRF1 from telomeres, enhancing telomerase-mediated telomere elongation. Tankyrase-1 multimerizes via its sterile alpha motif domain, but its functional implication remains elusive. Here, we found that excessive amounts of tankyrase-1 form punctate nuclear foci. This focus formation depends on both homophilic multimerization and heterophilic protein–protein interaction. These foci are functionally dormant because they do not efficiently release TRF1 from telomeres. Consistently, hyper-overexpression of tankyrase-1 attenuates its ability to elongate telomeres. These observations suggest that tankyrase-1 assembly to large protein complexes masks its telomeric function.

Structured summary:
MINT-7987689, MINT-7987677: *Tankyrase-1* (uniprotkb:O95271) and *TRF1* (uniprotkb:P54274) *colocalize* (MI:0403) by *fluorescence microscopy* (MI:0416)
MINT-7987977: *Tankyrase-1* (uniprotkb:O95271) *physically interacts* (MI:0915) with *TRF1* (uniprotkb:P54274) by *anti tag coimmunoprecipitation* (MI:0007)
MINT-7987998: *Tankyrase-1* (uniprotkb:O95271) *physically interacts* (MI:0915) with *Tankyrase-1* (uniprotkb:O95271) by *anti tag coimmunoprecipitation* (MI:0007).

1. Introduction

Tankyrase-1 poly(ADP-ribosyl)ates (PARsylates) a telomeric repeat-binding factor 1 (TRF1) [1]. PARsylated TRF1 dissociates from telomeres, resulting in an "open" state of telomeres. Thus, tankyrase-1 overexpression in human cells enhances telomere access of telomerase, which in turn elongates telomeres [2]. Since unusual maintenance of telomere length against the DNA end replication problem is an essential factor for cancer cell immortality, tankyrase-1 has been postulated as a target for cancer therapy [3,4].

Tankyrase-1 has five domains called ankyrin repeat cluster (ARC) I to V (see Fig. 3A), each of which works as an independent TRF1-binding unit [5,6]. Among them, ARC V is essential for TRF1 PARsylation [6]. Meanwhile, tankyrase-1 has a sterile alpha motif (SAM) domain, which contributes to protein multimerization [7,8]. Actually, tankyrase-1 forms large protein complexes (>2000 kDa) via the SAM domain both in vitro and in intact cells. In the cytoplasm, tankyrase-1 multimerization seems to be required for further assembly of punctate protein foci and larger vesicles, which presumably affect the apical secretion pathway [8]. However, the functional significance of tankyrase-1 multimerization in telomere length regulation is unknown. Here, we screened compounds that induce tankyrase-1 multimerization (i.e., nuclear focus formation), and found that hyper-overexpression of exogenous tankyrase-1 by histone deacetylase (HDAC) inhibitors leads to its focus formation in SAM- and ARC-dependent manners. Importantly, these foci were functionally inactive. This study demonstrates a novel regulation mechanism of tankyrase-1, which is distinct from modulation of the poly(ADP-ribose) polymerase (PARP) catalytic activity.

2. Materials and methods

2.1. Plasmids

The FLAG-nuclear localization signal (NLS)-tagged tankyrase-1 (FN-tankyrase-1) has been described [2]. Because more than half

Abbreviations: 3AB, 3-aminobenzamide; ARC, ankyrin repeat cluster; FN, FLAG tag and nuclear localization signal; HDAC, histone deacetylase; PARP, poly(ADP-ribose) polymerase; PARsylation, poly(ADP-ribosyl)ation; SAM, sterile alpha motif; TRF1, telomeric repeat-binding factor 1; TSA, trichostatin A; VPA, valproic acid

* Corresponding author. Fax: +81 3 3570 0484.
E-mail address: hseimiya@jfcr.or.jp (H. Seimiya).

0014-5793/$36.00 © 2010 Federation of European Biochemical Societies. Published by Elsevier B.V. All rights reserved.
doi:10.1016/j.febslet.2010.07.062

of endogenous tankyrase-1 resides outside the nucleus, NLS tagging to the exogenous gene allowed us to enhance the tankyrase-1 function exclusively in the nucleus [2]. FN-tank-ΔARC III-V and FN-tank-PARP-dead were constructed as described [6,9]. FN-tank-ΔSAM was generated by PCR with pLPC/FN-tankyrase-1 (Fig. 3A).

2.2. Fluorescence microscopy

Immunofluorescence staining was performed as described [10]. In brief, cells were transfected with each vector. After incubation for 20 h, cells were fixed with 2% paraformaldehyde and permeabilized with 0.5% Nonidet P-40. Cells were stained with anti-FLAG (M2) and anti-TRF1 (5747) [6]. For immuno-FISH, the permeabilized cells were hybridized with Cy3-PNA $(CCCTAA)_3$ [3] and stained with anti-FLAG.

2.3. Western blot analysis

Western blot analysis was performed as described [5] with anti-tankyrase-1 (H-350, Santa Cruz Biotechnology, Santa Cruz, CA), anti-glyceraldehyde-3-phosphate dehydrogenase (GAPDH) (10R-G109a), or anti-Myc (A-4, Santa Cruz Biotechnology).

2.4. Co-immunoprecipitation

TNE lysates [5] were incubated with anti-FLAG M2 affinity gel (Sigma-Aldrich, St. Louis, MO) for 1 h. After washing with the PARP reaction buffer [1], the bead-bound proteins were subjected to western blot analysis.

2.5. Southern blot analysis

FN-tankyrase-1-overexpressing HTC75 cells (HTC75/FN-tankyrase-1) [6] were treated with 125 nM trichostatin A (TSA) for up to 130 PD. Telomeric restriction fragments (TRF), which correspond to telomeric and subtelomeric DNAs, were detected by Southern blot analysis [6].

3. Results

3.1. HDAC inhibitors induce non-telomeric foci of exogenous tankyrase-1

Tankyrase-1 overexpression in the nuclei of HeLa I.2.11 cells eliminates the nuclear TRF1 dots, reflecting dissociation of TRF1 from telomeres and degradation of the protein (Fig. 1A, *top and middle*) [2,11]. In these cells, the exogenous tankyrase-1 exhibited flat nucleoplasmic distribution (Fig. 1A, *middle*). Treatment with 3-aminobenzamide (3AB, a PARP inhibitor) caused tankyrase-1 foci by tethering tankyrase-1 to the TRF1 dots (Fig. 1A, *bottom*) [3]. Thus, tankyrase-1 inhibition can be visualized by its focus formation.

To examine the mechanism for tankyrase-1 inhibition in intact cells, we screened the Screening Committee of Anticancer Drugs (SCADS) inhibitor kit, consisting of 95 function-defined inhibitors [12], for a compound that induces the tankyrase-1 foci. We found that HDAC inhibitors, Scriptaid and TSA, induce the foci (Fig. 1B, *Exp. 1*). This focus formation was also observed upon treatment with other structurally related (CHAHA) and unrelated [apicidin, valproic acid (VPA), MS-275, HC-toxin] HDAC inhibitors (Fig. 1B, *Exp. 2*; Supplementary Fig. 1), indicating that this effect was derived from HDAC inhibition. While these inhibitors blocked the TRF1 release from telomeres, the tankyrase-1 foci did not colocalize with TRF1 or telomeres (Fig. 1C and 2). These results suggest that HDAC inhibitors block the tankyrase-1 transgene in a different way than PARP inhibitors.

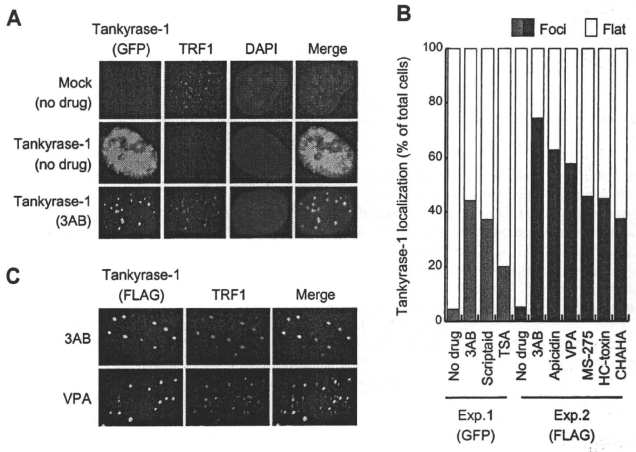

Fig. 1. Focus formation of exogenous tankyrase-1 by HDAC inhibitors. (A) Tankyrase-1–mediated dissociation of TRF1 from telomeres. HeLa I.2.11 cells were transfected with enhanced green fluorescence protein (EGFP)–FN-tankyrase-1 and incubated with or without PARP inhibitor 3AB (3 mM) for 18 h. Active tankyrase-1 exhibited flat nucleoplasmic distribution with the loss of telomeric TRF1 dots whereas 3AB induced telomeric co-localization of tankyrase-1 with TRF1. (B) Tankyrase-1 focus formation by HDAC inhibitors. Cells were transfected with EGFP–FN-tankyrase-1 (*Exp. 1*) or FN-tankyrase-1 (*Exp. 2*) and incubated with 3 mM 3AB, 1 μM Scriptaid, 100 nM TSA, 5 μM apicidin, 5 mM VPA, 5 μM MS-275, 0.5 μM HC-toxin, or 0.5 μM CHAHA for 18 h. These transgenes were expressed under the CMV promoter. More than 80 transfected cells were analyzed for each compound. (C) Confocal microscopy confirmed that tankyrase-1 foci by 3AB were telomeric whereas those by VPA were non-telomeric.

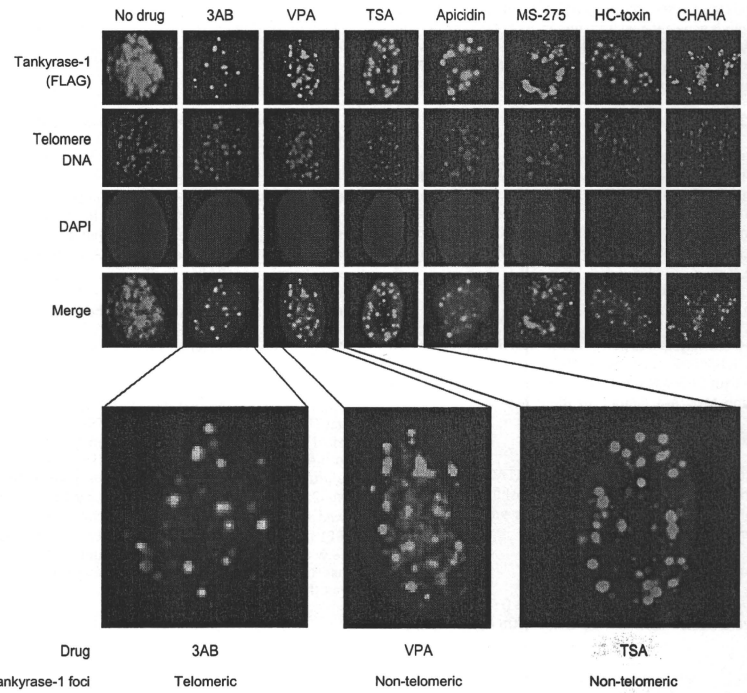

Fig. 2. Non-telomeric nuclear foci of exogenous tankyrase-1. HeLa I.2.11 cells were transfected with pLPC/FN-tankyrase-1 and incubated with the compounds for 18 h. Concentrations of the compounds were the same as in Fig. 1B. FN-tankyrase-1 and telomeres were detected by immuno-FISH.

3.2. HDAC inhibitors cause hyper-overexpression of CMV promoter-driven tankyrase-1

HDAC inhibitors might enhance tankyrase-1 acetylation, which in turn could disrupt the protein's function. However, we did not detect acetylated tankyrase-1 in HDAC inhibitor-treated cells (data not shown). HDAC inhibitors enhance gene expression driven by a CMV promoter [[13]; Okabe, S., Mashima, T., Seimiya, H., unpublished observation] that was used for the expression of the tankyrase-1 constructs in this study. Indeed, VPA and TSA significantly increased the expression of exogenous tankyrase-1 (Fig. 3B, *top panel*). This effect was specific, because it was not the case for 3AB. VPA and TSA also increased the level of endogenous tankyrase-1, but it was only marginal (Supplementary Fig. 2), supporting that HDAC inhibitors cause hyper-overexpression of the exogenous tankyrase-1.

3.3. Formation of non-telomeric tankyrase-1 foci requires SAM and ARC domains

Since tankyrase-1 multimerizes in its concentration-dependent manner [8], an elevated concentration of tankyrase-1 in the nucleus may lead to the self-association. If this were the case, the focus formation by HDAC inhibitors would be abolished by deletion of SAM domain. Actually, FN-tank-ΔSAM, which lost the ability to self-associate (Fig. 3A and C), did not form nuclear foci upon treatment with VPA or TSA (Fig. 4). This mutant retained hyper-overexpression upon treatment with the HDAC inhibitors (Fig. 3B). SAM domain is not sufficient to form large protein complexes in intact cells [8]. Thus, tankyrase-1 focus formation would need heterophilic protein interaction, in addition to SAM domain–mediated multimerization. So, we examined another mutant, FN-tank-ΔARC III-V, which lacks the C-terminal portion of ARCs (Fig. 3A and B). This mutant retained ARC I-II and SAM domains and thus could bind TRF1 and tankyrase-1, respectively (Fig. 3C). However, since this mutant lacks the essential ARC V for ligand PARsylation, it cannot elongate telomeres [6]. This mutant did not form nuclear foci upon treatment with HDAC inhibitors (Fig. 4). These observations indicate that tankyrase-1 focus formation involves both homophilic and heterophilic interactions via SAM and ARC domains, respectively. The catalytically inactive mutant FN-tank-PARP-dead (Fig. 3A) partially lost the ability to form the HDAC inhibitor-induced foci (Fig. 4), indicating that the focus formation occurs in PARP activity-dependent and -independent manners. SAM and ARC domains were also required for the focus formation by 3AB (Fig. 4).

Since HDAC inhibitors would also affect the expression of various genes, other proteins induced by HDAC inhibitors might be in-

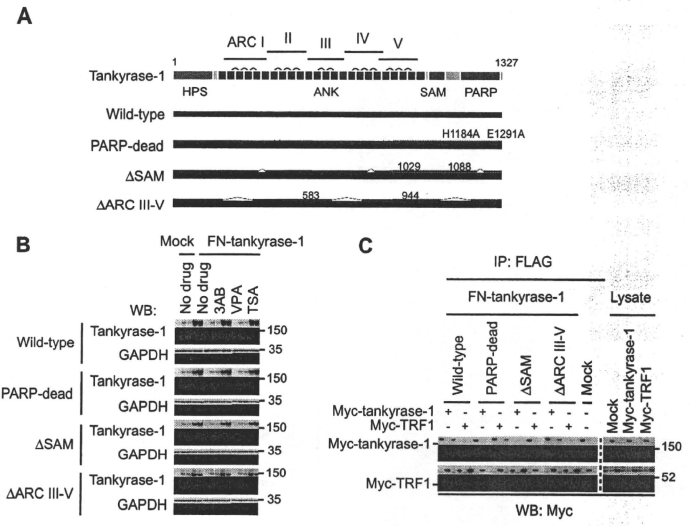

Fig. 3. HDAC inhibitors enhance expression of the tankyrase-1 transgenes. (A) FN-tankyrase-1 constructs used in the experiments. HPS, homopolymeric runs of His, Pro, and Ser. Bridges above two adjacent ankyrin repeats indicate the presence of a conserved histidine contributing to inter-repeat stabilization. These constructs contain a FLAG epitope tag and an NLS at the N-termini and are driven by a CMV promoter. Numbers indicate the positions of amino acid residues. (B) Hyper-induction of the tankyrase-1 transgenes by HDAC inhibitors. HeLa I.2.11 cells were transfected with each construct and incubated with the compounds overnight. The compound concentrations were the same as in Fig. 1B. The cell lysates were subjected to western blot analysis (WB). Numbers indicate the size markers. (C) Cells were transfected with FN-tankyrase-1 constructs and Myc-tankyrase-1 or Myc-TRF1. Cell lysates were subjected to immunoprecipitation (IP), followed by WB.

volved in the formation of tankyrase-1 foci. However, transfection with higher amounts of the plasmid, which elevated the expression level of the exogenous tankyrase-1, increased the frequency of spontaneous formation of the non-telomeric tankyrase-1 foci (data not shown). This result indicates that the excessive expression of tankyrase-1 causes its self-assembly.

3.4. Hyper-overexpression of tankyrase-1 attenuates its ability to elongate telomeres

It is likely that the multimerized tankyrase-1 foci, which did not eliminate the TRF1 dots in the nucleus, lost the ability to elongate telomeres. To examine this possibility, we continuously treated

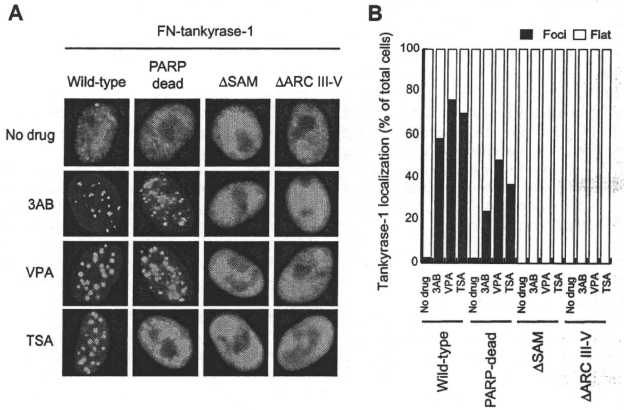

Fig. 4. Tankyrase-1 SAM and ARC domains mediate the focus formation. (A) HeLa I.2.11 cells were treated as in Fig. 3B and stained with anti-FLAG (*green*). DNA was counterstained by DAPI (*blue*). (B) Quantitative graph of the localization patterns of the tankyrase-1 constructs. More than 80 transfected cells were analyzed for each test.

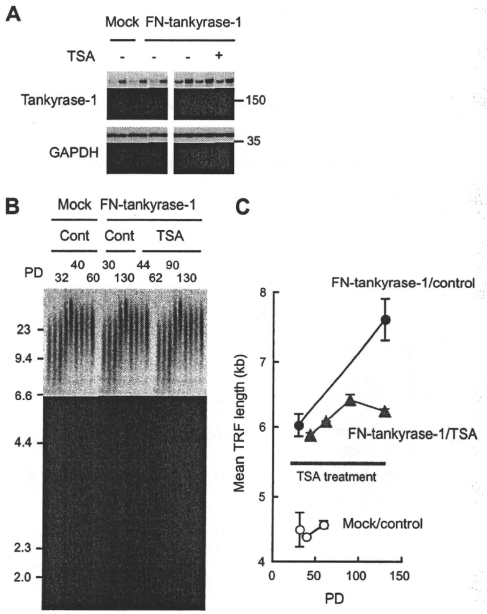

Fig. 5. Excessive tankyrase-1 attenuates its ability to elongate telomeres. HTC75/FN-tankyrase-1 cells at population doubling 22 (PD22) were treated with 125 nM TSA for up to 130 PD. (A) Western blot analysis. (B) Telomeric restriction fragments (TRF) detected by Southern blot analysis. Representative result of two experiments is shown. DNA size markers are indicated at the left (kb). (C) Graphic representations of telomere length change in (B).

HTC75/FN-tankyrase-1 cells [6], with a non-toxic dose (125 nM) of TSA. In these cells, FN-tankyrase-1 is stably overexpressed under the CMV promoter and further induced by TSA (Fig. 5A). While mock cells maintained the telomere length, HTC75/FN-tankyrase-1 cells elongated telomeres (Fig. 5B and C). As expected, TSA prevented efficient telomere elongation. TSA allowed moderate telomere elongation, which was consistent with the observation that TSA-treated cells exhibited a slight nucleoplasmic distribution of FN-tankyrase-1 (Figs. 2 and 4). TSA did not shorten telomeres in mock cells or inhibit telomerase activity in vitro (data not shown), indicating that HDAC inhibition has no detectable effect on the endogenous telomere maintenance machinery. We could not examine the effect of VPA on telomere length because chronic exposure to VPA was cytotoxic. These observations support that tankyrase-1 multimerization and subsequent larger protein complex formation block its telomeric function.

4. Discussion

Since tankyrase-1 expression is elevated in several cancers [14,15], it may play a role in carcinogenesis. This implies that tankyrase-1 could be a molecular target for cancer therapy. In fact, tankyrase-1 inhibition boosts the anticancer impact of a telomerase inhibitor [3]. Tankyrase-1 inhibition also induces synthetic lethality with BRCA-deficiency in multiple cancers [16]. Moreover, identification of tankyrases as axin-destabilizing proteins has opened the door for a therapy against Wnt signaling-dependent cancers [17].

Meanwhile, tankyrase-1-mediated down-regulation of TRF1 suppresses the mitotic abnormalities led by Aurora-A [9]. Namely, TRF1 mediates Aurora-A-induced occurrence of lagging chromosomes, resulting in tetraploidization of a cell [9]. Our present study suggests that too excessive up-regulation of tankyrase-1 may induce its focus formation and disturb, rather than enhance, TRF1 PARsylation. In that case, TRF1 would remain undegraded and mediate the Aurora-A-induced tetraploidization. Because tankyrase-1 and Aurora-A are frequently overexpressed in breast cancer [14,18], it would be interesting to determine the relationship between the expression levels of those proteins and ploidy alterations in such tumors.

Our finding that tankyrase-1 could be auto-regulated by forming dormant protein complexes would provide a novel clue for developing tankyrase inhibitors [17,19]. Thus, compounds that induce multimerization and focus formation of tankyrases may be utilized as functional inhibitors of the proteins. Such compounds would not affect PARsylation catalyzed by other PARPs and might be expected to exhibit a highly selective effect.

Acknowledgments

We thank Satoshi Tokunaga for assistance on Southern hybridization, laboratory members for discussion, and Screening Committee of Anticancer Drugs supported by Grant-in-Aid for Scientific Research on Priority Area "Cancer" from The Ministry of Education, Culture, Sports, Science and Technology, Japan for SCADS inhibitor kit. This work was funded by a Grant-in-Aid for

Scientific Research from the Ministry of Education, Culture, Sports, Science and Technology, Japan.

Appendix A. Supplementary data

Supplementary data associated with this article can be found, in the online version, at doi:10.1016/j.febslet.2010.07.062.

References

[1] Smith, S., Giriat, I., Schmitt, A. and de Lange, T. (1998) Tankyrase, a poly(ADP-ribose) polymerase at human telomeres. Science 282, 1484–1487.
[2] Smith, S. and de Lange, T. (2000) Tankyrase promotes telomere elongation in human cells. Curr. Biol. 10, 1299–1302.
[3] Seimiya, H., Muramatsu, Y., Ohishi, T. and Tsuruo, T. (2005) Tankyrase 1 as a target for telomere-directed molecular cancer therapeutics. Cancer Cell 7, 25–37.
[4] Seimiya, H. (2006) The telomeric PARP, tankyrases, as targets for cancer therapy. Br. J. Cancer 94, 341–345.
[5] Seimiya, H. and Smith, S. (2002) The telomeric poly(ADP-ribose) polymerase, tankyrase 1, contains multiple binding sites for telomeric repeat binding factor 1 (TRF1) and a novel acceptor, 182-kDa tankyrase-binding protein (TAB182). J. Biol. Chem. 277, 14116–14126.
[6] Seimiya, H., Muramatsu, Y., Smith, S. and Tsuruo, T. (2004) Functional subdomain in the ankyrin domain of tankyrase 1 required for poly(ADP-ribosyl)ation of TRF1 and telomere elongation. Mol. Cell Biol. 24, 1944–1955.
[7] Sbodio, J.I., Lodish, H.F. and Chi, N.W. (2002) Tankyrase-2 oligomerizes with tankyrase-1 and binds to both TRF1 (telomere-repeat-binding factor 1) and IRAP (insulin-responsive aminopeptidase). Biochem. J. 361, 451–459.
[8] De Rycker, M. and Price, C.M. (2004) Tankyrase polymerization is controlled by its sterile alpha motif and poly(ADP-ribose) polymerase domains. Mol. Cell Biol. 24, 9802–9812.
[9] Ohishi, T., Hirota, T., Tsuruo, T. and Seimiya, H. (2010) TRF1 mediates mitotic abnormalities induced by Aurora-A overexpression. Cancer Res. 70, 2041–2052.
[10] Ohishi, T., Tsuruo, T. and Seimiya, H. (2007) Evaluation of tankyrase inhibition in whole cells. Methods Mol. Biol. 405, 133–146.
[11] Chang, W., Dynek, J.N. and Smith, S. (2003) TRF1 is degraded by ubiquitin-mediated proteolysis after release from telomeres. Genes Dev. 17, 1328–1333.
[12] Kawada, M., Inoue, H., Masuda, T. and Ikeda, D. (2006) Insulin-like growth factor I secreted from prostate stromal cells mediates tumor-stromal cell interactions of prostate cancer. Cancer Res. 66, 4419–4425.
[13] Tanaka, J., Sadanari, H., Sato, H. and Fukuda, S. (1991) Sodium butyrate-inducible replication of human cytomegalovirus in a human epithelial cell line. Virology 185, 271–280.
[14] Gelmini, S., Poggesi, M., Distante, V., Bianchi, S., Simi, L., Luconi, M., et al. (2004) Tankyrase, a positive regulator of telomere elongation, is over expressed in human breast cancer. Cancer Lett. 216, 81–87.
[15] Xu, D., Zheng, C., Bergenbrant, S., Holm, G., Bjorkholm, M., Yi, Q., et al. (2001) Telomerase activity in plasma cell dyscrasias. Br. J. Cancer 84, 621–625.
[16] McCabe, N., Cerone, M.A., Ohishi, T., Seimiya, H., Lord, C.J. and Ashworth, A. (2009) Targeting Tankyrase 1 as a therapeutic strategy for BRCA-associated cancer. Oncogene 28, 1465–1470.
[17] Huang, S.M., Mishina, Y.M., Liu, S., Cheung, A., Stegmeier, F., Michaud, G.A., et al. (2009) Tankyrase inhibition stabilizes axin and antagonizes Wnt signalling. Nature 461, 614–620.
[18] Zhou, H., Kuang, J., Zhong, L., Kuo, W.L., Gray, J.W., Sahin, A., et al. (1998) Tumour amplified kinase STK15/BTAK induces centrosome amplification, aneuploidy and transformation. Nat. Genet. 20, 189–193.
[19] Yashiroda, Y., Okamoto, R., Hatsugai, K., Takemoto, Y., Goshima, N., Saito, T., et al. (2010) A novel yeast cell-based screen identifies flavone as a tankyrase inhibitor. Biochem. Biophys. Res. Commun. 394, 569–573.

VOLUME 28 · NUMBER 5 · FEBRUARY 10 2010

JOURNAL OF CLINICAL ONCOLOGY

ORIGINAL REPORT

Randomized Phase III Trial of Platinum-Doublet Chemotherapy Followed by Gefitinib Compared With Continued Platinum-Doublet Chemotherapy in Japanese Patients With Advanced Non–Small-Cell Lung Cancer: Results of a West Japan Thoracic Oncology Group Trial (WJTOG0203)

Koji Takeda, Toyoaki Hida, Tosiya Sato, Masahiko Ando, Takashi Seto, Miyako Satouchi, Yukito Ichinose, Nobuyuki Katakami, Nobuyuki Yamamoto, Shinzoh Kudoh, Jiichiro Sasaki, Kuoru Matsui, Koichi Takayama, Tatsuhiko Kashii, Yasuo Iwamoto, Toshiyuki Sawa, Isamu Okamoto, Takayasu Kurata, Kazuhiko Nakagawa, and Masahiro Fukuoka

See accompanying editorial on page 713 and article on page 744

A B S T R A C T

Purpose
Gefitinib is a small molecule inhibitor of the epidermal growth factor receptor tyrosine kinase. We conducted a phase III trial to evaluate whether gefitinib improves survival as sequential therapy after platinum-doublet chemotherapy in patients with advanced non–small-cell lung cancer (NSCLC).

Patients and Methods
Chemotherapy-naïve patients with advanced stage (IIIB/IV) NSCLC, Eastern Cooperative Oncology Group performance status of 0 to 1, and adequate organ function were randomly assigned to either platinum-doublet chemotherapy up to six cycles (arm A) or platinum-doublet chemotherapy for three cycles followed by gefitinib 250 mg orally once daily, until disease progression (arm B). Patients were stratified by disease stage, sex, histology, and chemotherapy regimens. The primary end point was overall survival; secondary end points included progression-free survival, tumor response, safety, and quality of life.

Results
Between March 2003 and May 2005, 604 patients were randomly assigned. There was a statistically significant improvement in progression-free survival in arm B (hazard ratio [HR], 0.68; 95% CI, 0.57 to 0.80; $P < .001$); however, overall survival results did not reach statistical significance (HR, 0.86; 95% CI, 0.72 to 1.03; $P = .11$). In an exploratory subset analysis of overall survival by histologic group, patients in arm B with adenocarcinoma did significantly better than patients in arm A with adenocarcinoma (n = 467; HR, 0.79; 95% CI, 0.65 to 0.98; $P = .03$).

Conclusion
This trial failed to meet the primary end point of OS in patients with NSCLC. The exploratory subset analyses demonstrate a possible survival prolongation for sequential therapy of gefitinib, especially for patients with adenocarcinoma.

J Clin Oncol 28:753-760. © 2009 by American Society of Clinical Oncology

From the Department of Clinical Oncology, Osaka City General Hospital; Department of Respiratory Medicine, Osaka City University Medical School, Osaka; Department of Thoracic Oncology, Aichi Cancer Center, Nagoya; Departments of Biostatistics and Preventive Services, Kyoto University School of Public Health, Kyoto; Department of Thoracic Oncology, National Kyushu Cancer Center; Department of Clinical Medicine, Faculty of Medical Science, Research Institute for Diseases of the Chest, Kyushu University, Fukuoka; Department of Thoracic Oncology, Hyogo Cancer Center, Akashi; Division of Respiratory Medicine, Kobe City General Hospital, Kobe; Division of Thoracic Oncology, Shizuoka Cancer Center, Nagaizumi; Department of Respiratory Medicine, Kumamoto University, Kumamoto; Department of Thoracic Malignancy, Osaka Prefectural Medical Center for Respiratory and Allergic Diseases, Habikino; Department Medical Oncology, Toyama University Hospital, Toyama; Department of Medical Oncology, Hiroshima City Hospital, Hiroshima; Department of Respiratory Medicine and Oncology, Gifu Municipal Hospital, Gifu; Department of Medical Oncology, Kinki University School of Medicine, Osaka-Sayama; Department of Cancer Chemotherapy Center, Osaka Medical College, Takatsuki; and the Kinki University School of Medicine, Sakai Hospital, Sakai, Japan.

Submitted April 23, 2009; accepted September 10, 2009; published online ahead of print at www.jco.org on December 28, 2009.

This study is registered with UMIN-CTR (http://www.umin.ac.jp/ctr/index.htm, identification number C000000035).

Authors' disclosures of potential conflicts of interest and author contributions are found at the end of this article.

Clinical Trials repository link available on JCO.org.

Corresponding author: Koji Takeda, MD, 2-13-22 Miyakojimahondohri, Miyakojima-ku, Osaka 534-0021, Japan; e-mail: kkk-take@ga2.so-net.ne.jp.

0732-183X/10/2805-753/$20.00

DOI: 10.1200/JCO.2009.23.3445

INTRODUCTION

Lung cancer is the most common cancer worldwide, with an estimated 1.2 million new cases globally (12.3% of all cancers) and 1.1 million deaths (17.8% of all cancer deaths) in 2000.[1] The estimated global incidence of non–small-cell lung cancer (NSCLC) in 2000 was approximately 1 million, which accounted for approximately 80% of all cases of lung cancer.[1] Treatment of advanced NSCLC is palliative; the aim is to prolong survival without leading to deterioration in quality of life.[2] The recommended first-line treatment of advanced NSCLC currently involves up to six cycles of platinum-based combination chemotherapy, with no single combination recommended over another.[3,4] Recently, combination chemotherapy of pemetrexed plus cisplatin was significantly superior to gemcitabine plus cisplatin in nonsquamous NSCLC.[5]

Gefitinib is an orally active epidermal growth factor receptor (EGFR) tyrosine kinase inhibitor (TKI) that blocks the signal transduction pathways

implicated in the proliferation and survival of cancer cells.[6] In two phase II trials in patients with pretreated advanced NSCLC (Iressa Dose Evaluation in Advanced Lung Cancer [IDEAL] 1 and 2), gefitinib 250 mg/d showed response rates of 12% and 18% and a median survival time (MST) of 7.0 and 7.6 months in IDEAL1 and 2, respectively; in addition, the toxicity profile was not severe.[7,8] This favorable tolerability profile, coupled with a mechanism of action that is distinct from that of cytotoxic agents, provides a strong rationale for use of gefitinib in combination with standard cytotoxic regimens. Platinum-doublet chemotherapy added to gefitinib in untreated patients with NSCLC was evaluated in two large-scale, placebo-controlled, randomized trials (INTACT-1 and -2).[9,10] Gefitinib showed no survival benefit over placebo when combined with standard platinum-doublet chemotherapy in both trials. Furthermore, gefitinib did not improve time to progression or objective tumor response over chemotherapy alone. These results were disappointing and surprising because of the significant antitumor activity of gefitinib when given alone to pretreated patients with NSCLC.

First, it is possible that each of the agents is working against a susceptible subpopulation of tumor cells so that the effect is redundant rather than additive, or that one agent results in the loss of an intermediary molecule that is essential to the function of the other agent, resulting in an antagonistic effect. Second, patients included in these studies were not selected on the basis of a specific biomarker, such as target EGFR expression, gene amplification, or mutations. Clinical profiles of females, never smokers, adenocarcinoma histology, and Asian ethnicity have all been recognized as favorable subgroups that respond to gefitinib.[11-14]

Because no additive effect was observed by administering gefitinib continuously in combination with chemotherapy, possible alternatives could be the administration of gefitinib in the interval between chemotherapy cycles or as sequential treatment after chemotherapy. This could also potentially prevent the problem of drug interference or antagonism. We conducted a randomized phase III trial to evaluate whether gefitinib improves survival as sequential therapy after platinum-doublet chemotherapy in chemotherapy-naive patents with NSCLC.

PATIENTS AND METHODS

Patients

Eligible patients were 20 to 75 years of age, with histologically or cytologically confirmed stage IIIB (with malignant pleural effusion or contralateral hilar lymph node metastases) or stage IV NSCLC who had not previously received any chemotherapy. Patients who had recurrence after complete surgical resection were permitted. Patients treated with either adjuvant or neoadjuvant chemotherapy were excluded in this trial. Additional criteria included a Eastern Cooperative Oncology Group performance status of 0 to 1, and adequate organ function as indicated by WBC count $\geq$ 4,000/μL, absolute neutrophil count $\geq$ 2,000/μL, hemoglobin $\geq$ 9.5 g/dL, platelets $\geq$ 100,000/μL, AST/ALT $\leq$ 2.5 times the upper limit of normal, total bilirubin $\leq$ 1.5 mg/dL, serum creatinine $\leq$ 1.2 mg/dL, and PaO_2 in arterial blood $\geq$ 70 mmHg. Asymptomatic brain metastases were allowed provided that they had been irradiated and were clinically and radiologically stable. Patients were excluded from the study if they had radiologically and clinically apparent interstitial pneumonitis or pulmonary fibrosis. All patients provided written informed consent, and the study protocol was approved by the West Japan Thoracic Oncology Group Protocol Review Committee and the institutional review board of each participating institution.

Treatment Plan

Eligible patients were centrally registered at West Japan Thoracic Oncology Group Data Center and were randomly assigned to receive either platinum-doublet chemotherapy up to six cycles (arm A) or three cycles of platinum doublet followed by gefitinib 250 mg/d orally, until disease progression (arm B). Patients who achieved disease control (response or stable disease) treated with three cycles of platinum-doublet went for gefitinib treatment phase in arm B. Each physician selected his/her chemotherapy options before randomization. Platinum-doublet chemotherapy options included any of the following: (1) carboplatin area under the curve 6, day 1, and paclitaxel 200 mg/m^2, day 1, every 3 weeks; (2) cisplatin 80 mg/m^2, day 1, and irinotecan 60 mg/m^2, days 1, 8, 15, every 4 weeks; (3) cisplatin 80 mg/m^2, day 1, and vinorelbine 25 mg/m^2, days 1, 8, every 3 weeks; (4) cisplatin 80 mg/m^2, day 1, and gemcitabine 1,000 mg/m^2 days 1, 8, every 3 weeks; or (5) cisplatin 80 mg/m^2, day 1, and docetaxel 60 mg/m^2 day 1, every 3 weeks. The dose of carboplatin was calculated using Calvert's formula, and the glomerular filtration rate was estimated by the Cockcroft-Gaut formula. These treatment schedules and doses are used as standard platinum-doublet regimens for advanced NSCLC in Japan.[15,16]

Randomization was stratified according to the institution, type of histology (adenocarcinoma *v* nonadenocarcinoma), clinical stage (IIIB *v* IV), and selected platinum-doublet regimens with the use of a minimization procedure. Patients receiving platinum-doublet chemotherapy received standard supportive treatments, including hydration and antiemetics, according to each institutional standard guideline. After withdrawing from the trial as a result of disease progression or intolerable toxicity, any systemic treatment, including with EGFR-TKI, was permitted in both arms.

Baseline and Follow-Up Assessments

Pretreatment evaluation included a complete medical history and physical examination, a CBC with differential and platelet count, standard biochemical profile, ECG, chest radiographs, computed tomography (CT) scans of the chest, abdomen, and brain, magnetic resonance imaging, and a whole-body bone scan. During treatment, a CBC and biochemical tests were performed at least every 2 weeks. A detailed medical history was taken and a complete physical examination with clinical assessment was performed every 2 weeks to assess disease symptoms and treatment toxicity, and chest

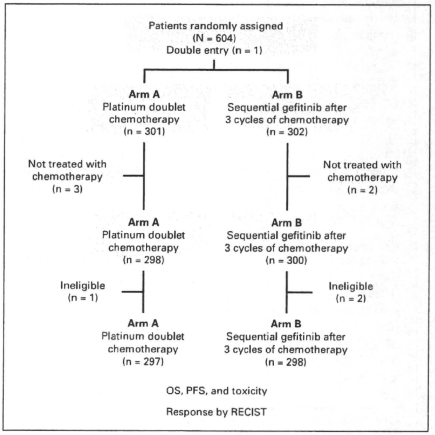

Fig 1. CONSORT diagram for the study. OS, overall survival; PFS, progression-free survival; RECIST, Response Evaluation Criteria in Solid Tumors.

radiographs were done every treatment cycle. Toxicity was evaluated according to the National Cancer Institute Cancer Common Toxicity Criteria (NCI-CTC) version2.[17]

All patients were assessed for response by CT scans monthly during treatment. Response Evaluation Criteria in Solid Tumors (RECIST) were used for the evaluation of response.[18]

Disease-related symptoms were assessed using the Lung Cancer Subscale (LCS) of the Functional Assessment of Cancer Therapy-Lung quality of life instrument (version 4.0).[19] Patients were asked to complete the instrument at the time of enrollment and at 12 weeks and 18 weeks after initiation of treatment. The maximum attainable score on the LCS was 28, where the patient was considered asymptomatic.

Statistical Analysis

The primary end point was OS; secondary end points included PFS, tumor response, safety, and quality of life. Based on previous trials evaluating platinum-doublet chemotherapy, the MST was approximately a range of 8 to 11 months.[3] In IDEAL-1, which was the trial of gefitinib alone in patients with previously treated NSCLC, median time to treatment failure was 98 days.[7] This trial was designed to detect a 3-month difference in MST. To attain 80% power at a two-sided significance level of .05, assuming a MST in the chemotherapy alone arm of 9 months with 2 years of follow-up after 3 years of accrual, 225 patients in each treatment group were required. Both the OS and PFS were estimated with the Kaplan-Meier method. Comparisons of OS and PFS between arms were assessed by the stratified log-rank test. Two interim analyses were planned after half the patients were registered and at the end of registration.

At the first interim analysis, 14% of patients in arm B unexpectedly withdrew from sequential gefitinib treatment after the three cycles of platinum-doublet chemotherapy at their own request because of hearing the news of interstitial lung disease (ILD) as a result of the use of gefitinib in Japan. If 15% of patients treated with sequential gefitinib withdrew, 284 patients in each arm were required to attain an 80% power at a two-sided significance level of .05, assuming a MST of the chemotherapy alone arm of 9 months with 2 years of follow-up after 3 years of accrual. Consequently, a protocol amendment was performed in April 2004.

For symptom analysis, comparisons of LCS between arms were conducted using a linear mixed-effects model in which the missing data depend on the observed LCS, using the MIXED procedure in SAS version 9 (SAS Institute, Cary, NC).

RESULTS

Patient Characteristics

From March 2003 to May 2005, 604 patients with advanced NSCLC from 39 institutions were enrolled (Appendix, online only). Patients were randomly assigned to platinum-doublet chemotherapy up to 6 cycles (n = 302, arm A) or sequential gefitinib after three cycles of platinum-doublet chemotherapy (n = 302, arm B). One patient was double entry in arm A, and three patients in arm A and two in arm B did not receive any chemotherapy. Therefore, a total of 598 patients (298 in arm A and 300 in arm B) were included in the analysis of patients' profiles and the assessment for toxicity. In addition, three patients did not meet the entry criteria; thus, 297 patients with measurable lesions by RECIST in arm A and 298 eligible patients in arm B were assessable for OS, PFS, and response. Figure 1 shows the CONSORT diagram. Table 1 presents baseline patient characteristics and lists the platinum-doublet chemotherapy regimen selected by each physician.

Table 1. Patients' Characteristics and Selected Platinum-Doublet Chemotherapy Regimens

Parameter	Arm A		Arm B		*P*
	No. of Patients	%	No. of Patients	%	
Patients enrolled	298		300		—
Median age, years	63		62		.114
Range	35-74		25-74		
Sex					
Male	191	34.6	192	64.0	.981
Female	107	67.8	108	36.0	
ECOG PS					
0	103	30.8	90	30.0	.778
1	195	69.2	210	70.0	
Histology					
Adenocarcinoma	232	77.9	237	79.0	.733
Nonadenocarcinoma	66	22.1	63	21.0	
Clinical stage					
IIIB	54	18.1	55	18.3	.946
IV	244	81.9	245	81.7	
Smoking status					
Smoker	202	67.8	210	70.0	.559
Nonsmoker	96	32.2	90	30.0	
Selected platinum-doublet chemotherapy regimens					
CP	193	64.8	195	65.0	.987
IP	8	2.7	10	3.3	
VP	44	14.8	45	15.0	
GP	45	15.1	42	14.0	
DP	8	2.7	8	2.7	

NOTE. Differences between two arms were tested by χ^2 test, excluding age (Wilcoxon test), ECOG PS.
Abbreviations: ECOG PS, Eastern Cooperative Oncology Group performance status; CP, carboplatin and paclitaxel; IP, irinotecan and cisplatin; VP, vinorelbine and cisplatin; GP, gemcitabine and cisplatin; DP, docetaxel and cisplatin.

Treatment Delivery

The median number of chemotherapy cycles was three (range, 1 to 6) in arm A, and three (range, 1 to 3) in arm B. One hundred seventy-two patients (57.3%) in arm B were treated with gefitinib after completion of three cycles of platinum-doublet. The median treatment duration of gefitinib was 69.5 days, and the maximum treatment duration was 1,324 days. As presented in Figure 2, EGFR-TKIs, which included gefitinib, erlotinib, and vandetanib, were used in 54.5% and 75.2% of patients in arm A and B, respectively, at any time during treatment of NSCLC. In arm B, gefitinib treatment did not take place because of early disease progression before the completion of three cycles of platinum-doublet chemotherapy in 93 patients (31.2%), and 33 (11.1%) in arm B rejected the use of gefitinib after platinum-doublet because of publication of a news report about gefitinib-induced ILD.

Treatment Efficacy

At the time of final analysis, 247 (83.2%) and 232 patients (78.0%) had died in arm A and arm B, respectively. The MST was 12.9 months for chemotherapy alone and 13.7 months for chemotherapy followed by gefitinib (hazard ratio [HR] according to Cox's regression model, 0.86; 95% CI, 0.72 to 1.03; $P = .11$ stratified log-rank test, Fig 3A). The PFS was 4.3 months in arm A and 4.6 months in arm B (HR, 0.68; 95% CI, 0.57 to 0.80; $P < .001$, Fig 3B).

When exploratory subset analysis were performed, sequential therapy with gefitinib after three cycles of platinum-doublet chemotherapy prolonged OS significantly in the subset of patients with adenocarcinoma (HR, 0.79; 95% CI, 0.65 to 0.98; $P = .03$; Fig 4A). There was no significant difference in OS due to the small subset of patients with nonadenocarcinoma (HR, 1.24; 95% CI, 0.85 to 1.79; $P = .25$; Fig 4B). In addition to the OS plots, the PFS plots for adenocarcinoma and nonadenocarcinoma were showed in Figure 4C and 4D, respectively. Furthermore, results of the subset analysis were summarized for forest plots in Figure 5. Another subset of smokers had a survival advantage with chemotherapy followed by gefitinib over chemotherapy alone. There was no difference between the two treatment groups in the subset of never smokers. Never smokers with NSCLC had a prolonged survival of about 23.5 months in arm A and 21.7 months in arm B.

The overall response rate was 29.3% for chemotherapy alone and 34.2% for chemotherapy followed by gefitinib. There was no significant difference between treatment arms ($P = .20$; Fisher's exact test). The overall disease control rate (response and stable disease) were 71.0% and 75.5% in arm A and in arm B, respectively ($P = .22$).

Toxicity

Toxicity was assessed according to NCI-CTC version 2 in all patients who received at least one treatment cycle of platinum-doublet chemotherapy (Table 2). Grade 3 or 4 anemia developed in 21.8% of patients in arm A and 13.3% of patients in arm B. There was a significant difference between the two arms ($P = .006$). Grade 3 or 4

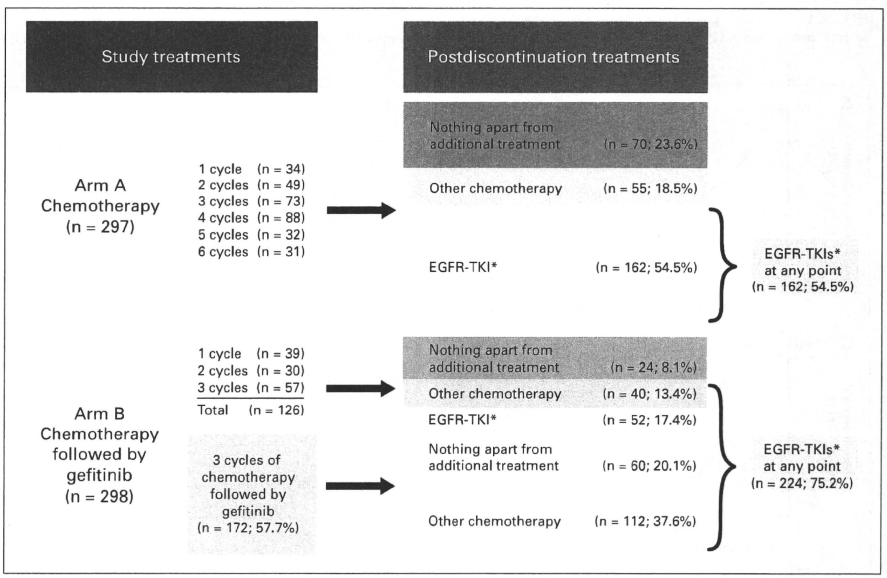

Fig 2. Exposure to active epidermal growth factor receptor tyrosine kinase inhibitor (EGFR-TKI), including postdiscontinuation treatments in the full analysis set population (n = 595).

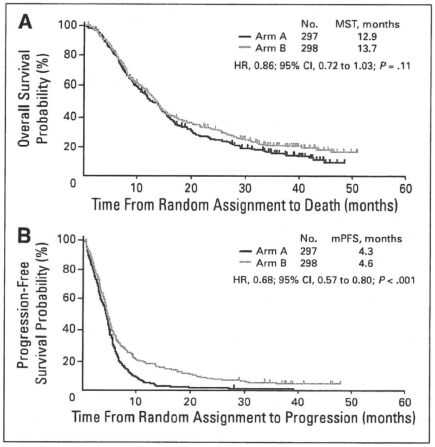

Fig 3. (A) Overall survival and (B) progression-free survival (n = 598). MST, median survival time; HR, hazard ratio; mPFS, median progression-free survival.

thrombocytopenia occurred in 10.7% of patients in arm A and 6.3% of patients in arm B, but differences did not reach significance ($P = .054$). Conversely, grade 3 or 4 AST/ALT elevation in arm B was severer than in arm A ($P = .002$). Severe ILD induced by gefitinib, which many patients feared developing, was observed in two patients in this study.

Disease-Related Symptoms Assessment

All 595 patients completed baseline LCS questionnaires; questionnaire completion rates were 81.0% at 12 weeks and 70.3% at 18 weeks. LCS data were missing in 111 surveys because of death or severe impairment of the patient's general condition; this accounted for 6.2% of the total number of surveys scheduled. The adjusted mean of initial summed scores of LCS were 20.3 for arm A and 20.6 for arm B, respectively. The adjusted LCS scores at 12 and 18 weeks were 21.0 and 20.9 for arm A, and 21.8 and 21.2 for arm B, respectively. Sequential gefitinib seemed to provide better symptom relief, although differences did not reach statistical significance ($P = .10$).

DISCUSSION

Sequential gefitinib therapy after three cycles of standard platinum-doublet chemotherapy showed no survival benefit over platinum-doublet chemotherapy up to six cycles in previously untreated patients with advanced NSCLC. However, sequential gefitinib was associated with significantly prolonged PFS. Recently, positive results with maintenance or sequential chemotherapy have been reported in clinical trials in PFS or time to progression; however, OS was not significantly lengthened.[20,21] More recently, pemetrexed administered to NSCLC patients without progression after four cycles of first-line treatment with platinum-doublet provided significant improvement in PFS compared with placebo (HR, 0.60; 95% CI, 0.49 to 0.73; $P < .00001$).[22]

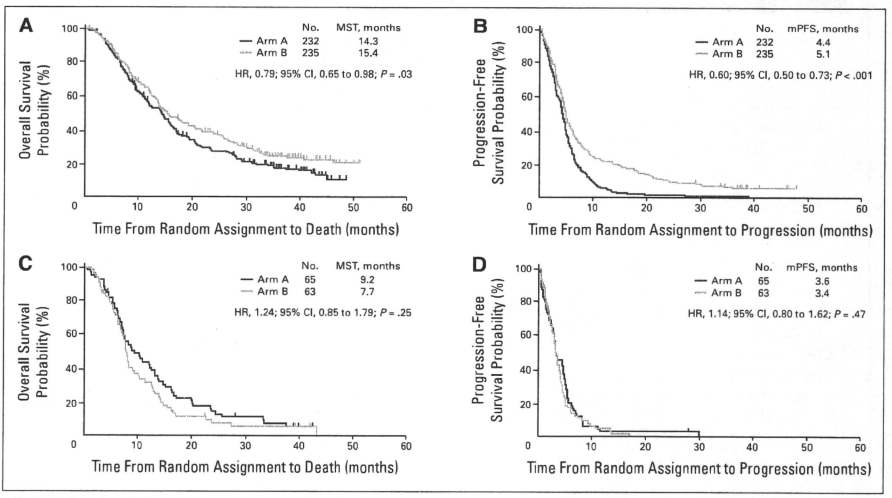

Fig 4. (A) Overall survival in the subset groups of patients with adenocarcinoma (n = 467), (B) progression-free survival in the subset groups of patients with adenocarcinoma (n = 467), (C) overall survival in the subset groups of patients with nonadenocarcinoma (n = 128), and (D) progression-free survival in the subset groups of patients with nonadenocarcinoma (n = 128). MST, median survival time; HR, hazard ratio; mPFS, median progression-free survival.

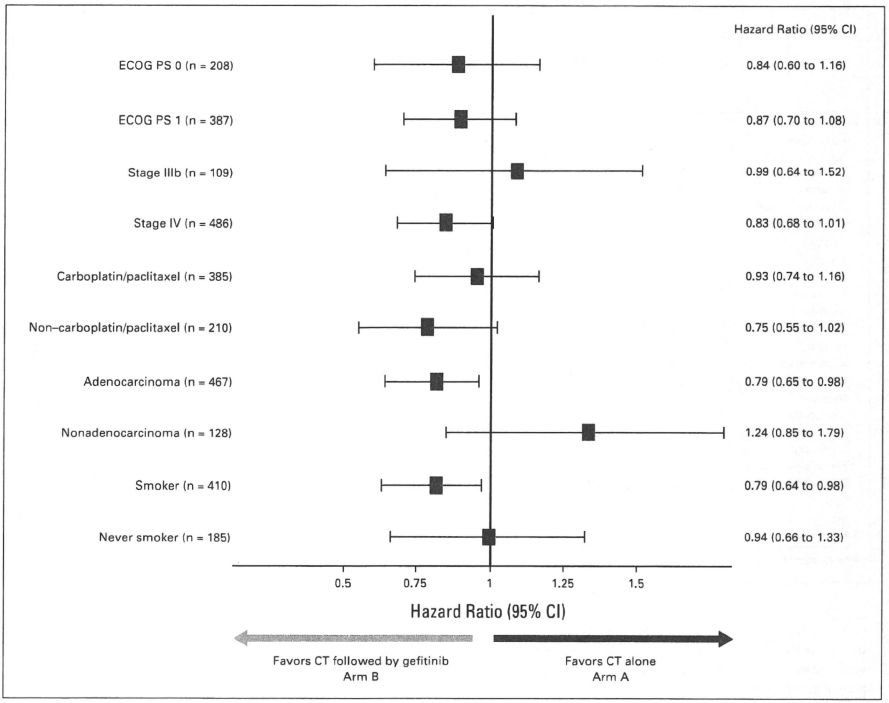

Fig 5. Forest plot subgroup analysis according to patients' backgrounds. CT, chemotherapy; ECOG PS, Eastern Cooperative Oncology Group performance status.

It was the first randomized, double-blind, placebo controlled trial to demonstrate a significant OS prolongation for maintenance treatment with pemetrexed in patients with advanced NSCLC (HR, 0.79; 95% CI, 0.65 to 0.95; $P = .012$).[22] The results of the Sequential Erlotinib in Unresectable NSCLC (SATURN) study, which was a randomized, double-blind, placebo controlled trial with erlotinib as maintenance, were presented this year. Erlotinib maintenance treatment had improvement in PFS of 41% compared with placebo.[23] Maintenance or sequential chemotherapy strategy after standard treatment has lately been receiving considerable attention. As a result, our trial was considered a consolidation therapy using other agent without progression after front-line treatment rather than maintenance.

Although the median number of chemotherapy cycles was three in both arms, 47.5% of patients received more than four cycles in Arm A. The number of treatment cycles was lower in Japanese than in whites; however, comparability was to be kept between the two arms in this randomized trial. These results were consistent with Japanese data on the median number of cycles of platinum-doublet chemotherapy.[15]

Toxicity results were consistent with previous Japanese studies of advanced NSCLC patients who received platinum-doublet chemotherapy.[15,16] Furthermore, no significant severe adverse events were seen that were not predictable from the safety profiles of gefitinib in sequential therapy after platinum-doublet chemotherapy. Recently published data suggested that gefitinib might be associated with ILD in Japanese patients[11]; however, in our study, the overall incidence of ILD was less than 1%, and no imbalance was identified between the two treatment arms in terms of ILD.

It was interesting that sequential gefitinib therapy had a significant survival prolongation in patients with adenocarcinoma histology (HR, 0.79; 95% CI, 0.65 to 0.98; $P = .03$). There was no difference also in PFS or OS for patients with nonadenocarcinoma. It was possible that these patients just did not benefit from an ineffective therapy of sequential gefitinib. In patients with NSCLC, adenocarcinoma histology, nonsmoker, and Japanese or Asian ethnicity are favorable predictive factors for a response to gefitinib treatment.[11-14] When the analysis was performed in the most favorable subset population that responded to gefitinib—that is, among those with both adenocarcinoma histology and nonsmokers—the MST was 23.5 months in arm A and 25.1 months and in arm B, respectively. Indeed, more than three quarters of the patients with favorable profiles in arm A received gefitinib after the protocol treatment, because physicians recognized

Table 2. Toxicity According to National Cancer Institute Common Toxicity Criteria Version 2

	Arm A (n = 298)				Arm B (n = 300)				
	Grade 3		Grade 4		Grade 3		Grade 4		
Toxicity	No.	%	No.	%	No.	%	No.	%	χ^2 Test *P* for Grade 3 + 4
Hematologic									
Leukopenia	98	32.9	21	7.0	97	32.3	14	4.7	.461
Neutropenia	90	30.2	136	45.6	79	26.3	133	44.3	.153
Febrile neutropenia	33	11.1	5	1.7	38	12.8	0	0	.297
Anemia	57	19.1	8	2.7	35	11.7	5	1.7	.006
Thrombocytopenia	32	10.7	0	0	18	6.0	1	0.3	.054
Nonhematologic									
Anorexia	43	14.4	0	0	33	11.0	2	0.7	.316
AST/ALT	11	3.7	1	0.3	32	10.7	0	0	.002
Constipation	25	8.4	0	0	20	6.7	1	0.3	.631
Creatinine	1	0.3	0	0	0	0	0	0	.315
Diarrhea	6	2.0	0	0	5	1.7	0	0	.152
Dyspnea	3	1.0	5	1.7	4	1.3	5	1.7	.816
Fatigue	22	7.4	7	2.3	18	6.0	4	1.3	.294
Hypersensitivity	1	0.3	1	0.3	2	0.7	2	0.7	.417
Infection	36	12.1	1	0.3	26	8.7	0	0	.135
Nausea	38	12.8	0	0	29	9.7	0	0	.232
Neuropathy									
Motor	5	1.7	1	0.3	4	1.3	1	0.3	.991
Sensory	12	4.0	1	0.3	7	2.3	0	0	.260
Performance status	27	9.1	8	2.7	23	7.7	9	3.0	.676
Pneumonitis (ILD)	2	0.7	0	0	4	1.3	0	0	.417
Rash	2	0.7	0	0	1	0.3	0	0	.559
Stomatitis/pharingitis	0	0	0	0	2	0.7	0	0	.482
Vomiting	12	4.0	1	0.3	15	5.0	2	0.7	.465

Abbreviation: ILD, interstitial lung disease.

these patients were more likely to respond to gefitinib. Patients who were nonsmokers with adenocarcinoma in arm A resulted in subsequent gefitinib therapy as well as in arm B.

Activating mutations in the gene for *EGFR* appear in a subset of adenocarcinoma of lung cancer.[24,25] A higher response to EGFR-TKIs is noted in specific subgroups that include females, never smokers, patients with adenocarcinoma histology, and East Asians.[12] Higher EGFR mutation rates are also noted in these subgroups and are also related to a better response to EGFR-TKIs[24,25] and longer survival.[12] Patients with these mutations exhibit objective response rates in the range of 75% to 95%.[12-14,26,27]

Patients included in this study were not selected on the basis of the target *EGFR* mutation status, because when this study was planned, we had not recognized the *EGFR* mutation as a predictive factor to respond to gefitinib. In Japanese patients with adenocarcinoma, a higher incidence of *EFGR* mutations, are estimated compared with white patients. It seems that more than 40% of Japanese patients with adenocarcinoma have an *EGFR* mutation.[12] Complex results in this study can be explained by analyzing the *EGFR* mutation status of participating patients. It may be important to select patients who are known to receive a clinical benefit with treatment using an EGFR-TKI.

In conclusion, this trial failed to meet the primary end point of OS in patients with advanced NSCLC. The exploratory subset analyses demonstrate a possible survival prolongation for sequential therapy of gefitinib, especially for patients with adenocarcinoma. Further investigations are warranted to confirm the best sequential therapy after platinum-based chemotherapy for patients with advanced NSCLC.

AUTHORS' DISCLOSURES OF POTENTIAL CONFLICTS OF INTEREST

Although all authors completed the disclosure declaration, the following author(s) indicated a financial or other interest that is relevant to the subject matter under consideration in this article. Certain relationships marked with a "U" are those for which no compensation was received; those relationships marked with a "C" were compensated. For a detailed description of the disclosure categories, or for more information about ASCO's conflict of interest policy, please refer to the Author Disclosure Declaration and the Disclosures of Potential Conflicts of Interest section in Information for Contributors.

Employment or Leadership Position: None **Consultant or Advisory Role:** Takayasu Kurata, Takeda Pharmaceutical (U) **Stock Ownership:** None **Honoraria:** Miyako Satouchi, AstraZeneca; Yukito Ichinose, AstraZeneca; Nobuyuki Yamamoto, AstraZeneca; Takayasu Kurata, AstraZeneca, Eli Lilly; Kazuhiko Nakagawa, AstraZeneca, sanofi-aventis; Masahiro Fukuoka, AstraZeneca, Chugai Pharmaceutical **Research Funding:** None **Expert Testimony:** None **Other Remuneration:** None

AUTHOR CONTRIBUTIONS

Conception and design: Koji Takeda, Toyoaki Hida, Masahiko Ando, Miyako Satouchi, Nobuyuki Yamamoto, Takayasu Kurata, Kazuhiko Nakagawa, Masahiro Fukuoka

